An analytical model for a cylindrical reacting dissipative muffler

M. Pachebat[1], E. Portier[2], Y. Auregan[3]

1: Société d'Acoustique Industrielle, Parc d'activité du Moulin de Massy, 1 rue du Saule Trapu, 91882 MASSY
2: Centre de Transfert de Technologies du Mans, 20 rue Thalès de Milet, 72000 Le Mans
3: Laboratoire d'Acoustique de l'Université du Maine, UMR CNRS 6613, Av. Olivier Messiaen, 72085 LE MANS

Abstract: An analytical model is developed which can be used to predict the acoustic performance of a reacting dissipative muffler at low frequencies with flow. Predictions are compared with measurements, illustrating effects of mean flow, acoustic impedance of the perforated screen, level of acoustic excitation and geometry on the scattering matrix of the silencer.

Keywords: analytical model, reacting muffler, scattering matrix, hydrodynamic modes, impedance model, non-linear effects

1. Introduction

The cylindrical dissipative silencer is one of the most common devices in practical flow duct acoustics and especially in automotive applications [1]. Its acoustic performance can be predicted in the general case by a FEM approach or by mode matching techniques. However, in practical situations, reactive muffler devices used for transportation vehicles or industry engines are frequently exposed to high sound pressure levels and high flow rate and these methods require a considerable numerical effort limiting their use in practice. Furthermore only few data in the literature can be used to illustrate clearly the effect of mean flow on the complete scattering matrix coefficients of such mufflers.

In this paper, an analytical model is developed, starting from a very versatile model based on a continuous approach [2]. A modified version is exposed (section 2) which can be used to predict the acoustic performance – i.e. the scattering matrix - of a reacting dissipative muffler at low frequencies with flow and/or finite amplitude effects. The key point of this model is to take into account the radial variation of pressure on either side of the inner perforated tube and to include the coupling of evanescent modes of two consecutive discontinuities. This approach can overcome numerical difficulties usually encountered with models based on segmentation technique [3][4]. It can take into account highly porous screens and/or porous materials including with high flow resistivity. The effect of flow on acoustic impedance is still an open issue [5]. Flow and non-linear effects are described (section 3) by means of an impedance model [6]. After a presentation of the experimental set-up (section 4), the scattering matrix of the muffler is compared to measurements in several configurations (section 5): simple expansion chamber, with either a perforated tube with a wire mesh or a flow, quarter wave resonators, and high sound pressure level.

2. Analytical model

The extension by Y. Auregan [7] of the analytical model [2] in order to take into account fluid flow and hydrodynamic modes is presented hereafter.

2.1 Formulation of the problem

We consider a geometry consisting in an inner cylinder with radius r_a^*, referred to as region A, and of an outer coaxial cylinder with radius varying from r_a^* to r_b^*, referred to as region B (Figure 1). The fluid is at rest in the outer cylinder and a supposed uniform flow of mean velocity U_0 is present in the inner cylinder. Between those two regions, a rigid perforated screen induces a pressure jump.

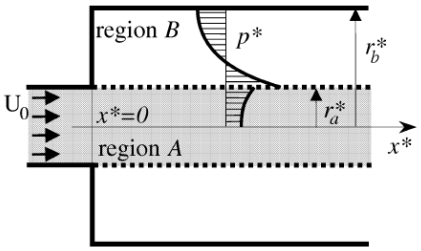

Figure 1 : Geometry – Pressure Profile

The fluctuating variables used here are the pressure p^*, the axial velocity u^* and radial velocity v^* with a subscript *a* or *b* depending on the region. The fluid is characterized by the density ρ_0 and the adiabatic sound velocity c_0. For a harmonic motion, solutions are in the general form $q^*(x^*, r^*, t^*) = q^*(r^*)e^{j(wt^* - K^* x^*)}$ with $q^* = p^*, u^*, v^*$. Dimensionless variables are used: $t = w.t^*$, $K = c_0 K^*/w$, $x = w.x^*/c_0$, $r = w.r^*/c_0$, $p = p^*/\rho_0 c_0^2$, $u = u^*/c_0$, $v = v^*/c_0$.

2.2 Mean propagation equations on both regions

Using the propagation equations and integrating them in both regions over the transversal dimension, the following averaged equations are obtained:

$$\left[(1-KM_a)^2 - K^2\right]P_a + y_a P_a' = 0, \qquad [1]$$

$$\left[1-K^2\right]P_b - y_b P_b' = 0, \qquad [2]$$

where P_i is the mean pressure over the section $S_{a,b}$ ($S_a = \pi.r_a^2$ and $S_b = \pi.(r_b^2 - r_a^2)$), P'_i is the value of $\partial p_i/\partial r$ at $r=r_a$, $y_a = 2\pi r_a/S_a$, $y_b = 2\pi r_b/S_b$ and $M_a=U_0/c_0$.

2.3 Radial acoustic displacement continuity

The continuity of the radial acoustic displacement at the interface of the two regions yields:

$$P_a^{'} = (1-KM_a)^2 P_b^{'}. \qquad [3]$$

2.4 Pressure gap at the interface

With a perforated screen of dimensionless impedance Z_S the pressure jumps from $p_b(r_a)$ to $p_a(r_a)$ with:

$$p_a(r_a) - p_b(r_a) = jZ_s P_b^{'}. \qquad [4]$$

2.5 Pressure profiles

In this paper, the pressure profile is approximated by a shape with two degrees of freedom, i.e. $p_a(r) = p_a(0) + A.r^2$. This yield to write the pressure in the region A for $r=r_a$:

$$p_a(r_a) = P_a + \delta_a P_a^{'}. \qquad [5]$$

with $\delta_a = r_a/4$.

In a similar way, the value of the pressure in the region B for $r=r_a$ is given by:

$$p_b(r_a) = P_b - \delta_b P_b^{'}, \qquad [6]$$

where $\delta_b = f(\alpha).r_a$ and $f(\alpha) = \dfrac{(1-\alpha)(3+\alpha)}{3(1+\alpha)^2}$

2.6 Dispersion equation

The equations [1] to [6] can be written in the form :

$$\begin{pmatrix} (1-KM_a)^2 & 0 & y_a(1-KM_a)^2 \\ 0 & 1-K^2 & -y_b \\ 1 & -1 & (1-KM_a)^2\delta_a + \delta_b - jZ_s \end{pmatrix} \begin{pmatrix} P_a \\ P_b \\ P_b^{'} \end{pmatrix} = \begin{pmatrix} 0 \\ 0 \\ 0 \end{pmatrix} \qquad [7]$$

The determinant of the system must vanish to have non trivial solution. This gives the dispersion equation for the dimensionless wavenumber K:

$$\begin{aligned} &\left[(1-KM_a)^2\delta_a + \delta_b - jZ_s\right]\left[(1-KM_a)^2 - K^2\right]\left[1-K^2\right] \\ &- y_b\left[(1-KM_a)^2 - K^2\right] - y_a(1-KM_a)^2\left[1-K^2\right] = 0. \end{aligned} \qquad [8]$$

This egenequation is a sixth order equation with flow that reduces to four without flow [2]:

$$(1-K^2)\left[(1-K^2)(\delta_a + \delta_b - jZ_s) - y_a - y_b\right] = 0. \qquad [9]$$

Without flow, the analytical solutions are :

$$K_{1,2} = \pm 1,$$
$$and K_{3,4} = \pm\sqrt{1 - \frac{y_a + y_b}{\delta_a + \delta_{bS}}}, \qquad [10]$$

where $\delta_{bS} = \delta_b - jZ_S$.

With flow, the solutions are easily evaluated numerically. There behaviour have to be carefully identified and this is detailed in the following section.

2.7 Modes behaviour

Without screen, e.g. a simple expansion chamber, the dispersion equation being real, three pairs of complex conjugate or real solutions are obtained.

The two first one numbered **1** and **2** on Figure 2 are real and closed to $K_1 = 1/(1+M_{av})$ and $K_2 = -1/(1-M_{av})$ where the mean Mach number is $M_{av} = S_a M_a/(S_a + S_b)$. They are referred to as "quasi-planar modes". Solutions **3** and **4** are close to the imaginary axis and are referred to as "higher-order modes". The two last modes **5** and **6** are close to the value $(1 \pm j)/M_a$ and are the hydrodynamic or vorticity modes.

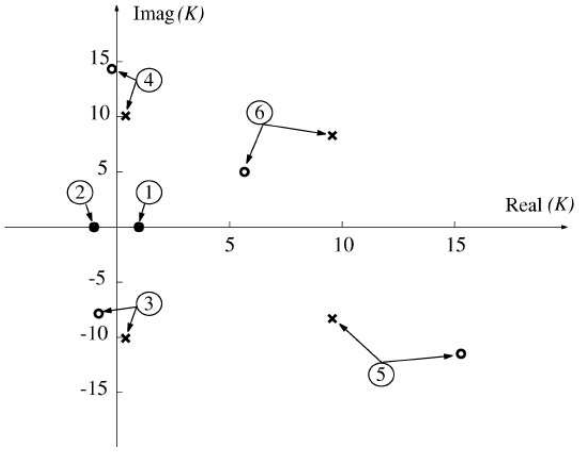

Figure 2 : Roots of the dispersion equation (from [7])
x : without screen, o : with sreen

Auregan [7] proposed the use of the Briggs criterion to sort the modes by their direction of propagation and to study their stability. Thus the modes **2** and **4** are upstream propagating waves, and the mode **4**, with positive imaginary part is attenuated with the distance, i.e. an evanescent mode. The modes **1**, **3**, **5** and **6** are downstream propagating waves, the modes **3** and **5** are evanescent (negative imaginary parts) and the mode **6**, on the opposite, is unstable due to its positive imaginary part. The mode **6** is relevant to the vortex shedding with amplitude that grows with the propagation. In some case, if the frequency of the vortex shedding matches with the length cavity, a whistling can occur. This particular point is not further detailed in the following but it is in theory in the scope of the model.

With a resistive screen, the dispersion equation is no longer real. As a consequence, the acoustic modes **1** and **2** are no longer real and a very small imaginary part appears. Furthermore, the imaginary part of mode **6** decreases (Figure 2) which means

that this hydrodynamic mode is less unstable with a screen.

2.8 Mean acoustic quantities

When the solutions of the dispersion equation are computed and correctly sorted, the acoustic pressure and velocity are written in each region.

In the region A, the acoustic pressure is:

$$P_a(x) = \sum_m P_m e^{-jK_m x}, \qquad [11]$$

m is the mode number, and the acoustic velocity is given by the use of the axial Euler equation $j(1-KM_a)U_a = -\partial P_a/\partial x$:

$$U_a(x) = \sum_m \frac{K_m}{1-K_m M_a} P_m e^{-jK_m x}. \qquad [12]$$

In the region B, the acoustic quantities are obtained with the following eigenfunctions for the mode number *m* $P_{bm} = s_m P_{am}$ and $P'_{bm} = t_m P_{am}$:

$$t_m = -\frac{(1-K_m M_a)^2 - K_m^2}{y_a (1-K_m M_a)^2}, \qquad [13]$$

$$s_m = \frac{y_b}{1-K_m^2} t_m = -\frac{y_b}{y_a} \frac{(1-K_m M_a)^2 - K_m^2}{(1-K_m^2)(1-K_m M_a)^2}. \qquad [14]$$

Thus the acoustic pressure in the region B is:

$$P_b(x) = \sum_m s_m P_m e^{-jK_m x}, \qquad [15]$$

and the acoustic velocity is obtained with the axial Euler equation in this region $jU_b = -\partial P_b/\partial x$:

$$U_b(x) = \sum_m s_m K_m P_m e^{-jK_m x}. \qquad [16]$$

An additional quantity, the radial displacement ξ_s at $r=r_a$ is given by:

$$\xi_S(x) = \sum -t_m P_m e^{-jK_m x}. \qquad [17]$$

2.9 Boundary conditions

The geometry of the muffler used in this paper is described on Figure 3. Two cavities of respective length L_1 and L_2 are added at each extremity of a perforated tube. These two cavities are provided to give a kind of quarter wave response to the muffler.

A decomposition of incoming and outcoming waves is used at both side of the perforated zone directly related to the modes previously defined.

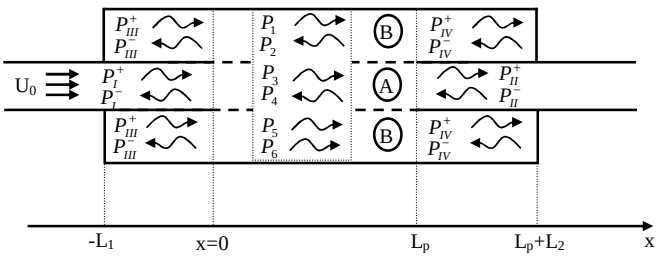

Figure 3 : Muffler design

A set of boundary conditions is obtained with the continuity of the mean pressure and the mean velocity at the sudden expansion and then at the sudden contraction. These boundary conditions are detailed in the tables 1 and 2.

	Kind of continuity	Expansion (x=0)
Region A	Pressure	$P_I^+ + P_I^- = \sum_m P_m$
	Velocity	$P_I^+ - P_I^- = \sum_m \frac{K_m}{1-K_m M_a} P_m$
Region B	Pressure	$P_{III}^+ + P_{III}^- = \sum_m s_m P_m$
	Velocity	$P_{III}^+ - P_{III}^- = \sum_m s_m K_m P_m$

Table 1 : Boundary conditions at the expansion

	Kind of continuity	Contraction (x=Lp)
Region A	Pressure	$P_{II}^+ + P_{II}^- = \sum_m P_m e^{-jK_m L_p}$
	Velocity	$P_{II}^+ - P_{II}^- = \sum_m \frac{K_m}{1-K_m M_a} P_m e^{-jK_m L_p}$
Region B	Pressure	$P_{IV}^+ + P_{IV}^- = \sum_m s_m P_m e^{-jK_m L_p}$
	Velocity	$P_{IV}^+ - P_{IV}^- = \sum_m s_m K_m P_m e^{-jK_m L_p}$

Table 2 : Boundary conditions at the contraction

Two new boundary conditions appear in presence of flow. They are linked to the Kutta condition which states that any particle leaves tangentially the trailing edge. That leads to a radial particle displacement ξ_s and its derivative null at the interface (Table 3).

Kind of continuity	Expansion (x=0)
Null radial displacement	$0 = \sum_m t_m P_m$
Null derivative	$0 = \sum_m t_m K_m P_m$

Table 3 : Kutta's Boundary conditions at expansion

2.10 Scattering matrix of the muffler

The quarter wave cavities are introduced in the model with the reflection coefficient at the back of the cavities:

- $R_1 = P_{III}^+ / P_{III}^-$ and $R_1 = e^{-2jL_1}$.
- $R_2 = P_{IV}^- / P_{IV}^+$ and $R_2 = e^{-2jL_2}$.

The previous boundary conditions and the presence of the quarter wave cavities yield to the following matrix relation:

$$[M_1]X_1 = [M_2]X_2 \qquad [18]$$

with :

$$[M_1]=\begin{bmatrix}1&0\\1&0\\0&1\\0&1\\0&0\\0&0\\0&0\\0&0\\0&0\\0&0\end{bmatrix},\quad X_1=\begin{pmatrix}P_I^+\\P_{II}^-\end{pmatrix},\quad X_2=\begin{bmatrix}P_{II}^+\\P_I^-\\P_1\\P_2\\P_3\\P_4\\P_5\\P_6\\P_{III}^-\\P_{IV}^+\end{bmatrix}$$ and

$$[M_2]=\begin{bmatrix}0&-1&1&1&1&1&1&1&0&0\\0&1&A_1&A_2&A_3&A_4&A_5&A_6&0&0\\-1&0&E_1&E_2&E_3&E_4&E_5&0&0&0\\1&0&-A_1E_1&-A_2E_2&-A_3E_3&-A_4E_4&-A_5E_5&0&0&0\\0&0&s_1&s_2&s_3&s_4&s_5&s_6&-(R_1+1)&0\\0&0&s_1K_1&s_2K_2&s_3K_3&s_4K_4&s_5K_5&s_6K_6&-(R_1-1)&0\\0&0&s_1E_1&s_2E_2&s_3E_3&s_4E_4&s_5E_5&0&0&-(R_2+1)\\0&0&s_1K_1E_1&s_2K_2E_2&s_3K_3E_3&s_4K_4E_4&s_5K_5E_5&0&0&-(1-R_2)\\0&0&t_1&t_2&t_3&t_4&t_5&t_6&0&0\\0&0&t_1K_1&t_2K_2&t_3K_3&t_4K_4&t_5K_5&t_6K_6&0&0\end{bmatrix}$$

where $E_m=e^{-jK_mL_p}$ and $A_m=K_m/(1-K_mM_a)$.
The equation [18] can be written :

$$X_2=inv[M_2].[M_1].X_1.$$
$$X_2=[M].X_1. \qquad [19]$$

Finally the first four elements of the matrix $[M]$ are the scattering matrix.

3. Surface Impedance Model

The previous model is based on the surface impedance which links the pressure gap at the interface of the perforated screen to the acoustic velocity (equation [4]).
The impedance model used in this paper is the one proposed by Elnady [6]. In addition to the classical linear model – i.e. that consider the viscosity, the radiation, the end corrections and the grazing flow – the impedance model consider the interaction between holes of a perforated plate and the non-linear effect due to high sound pressure level.

3.1 Linear model impedance

The linear model used for the resistance *r* and the reactance χ is given by:

$$\begin{cases} r=\mathrm{Re}\left\{\frac{jk}{\sigma C_D}\left[\frac{e}{F(\mu')}+\frac{\delta_{re}}{F(\mu)}f_{\mathrm{int}}\right]\right\}+\frac{1}{\sigma}\left[1-\frac{2J_1(kd)}{kd}\right]+\frac{0.5}{\sigma}M_r+\frac{1.15}{\sigma C_D}M_t, \\ \chi=\mathrm{Im}\left\{\frac{jk}{\sigma C_D}\left[\frac{e}{F(\mu')}+\frac{0.5d}{F(\mu)}f_{\mathrm{int}}\right]\right\}-\frac{0.3}{\sigma}M_r. \end{cases} \qquad [20]$$

The first terms of impedance (resistance and reactance) correspond to the viscosity, the end correction and the interaction between holes effects. The second term of the resistance corresponds to the radiation effect. The third term of the resistance and the second of the reactance correspond to the consideration of grazing flow. The last term of the resistance is relevant to a through flow, if present.

The parameters of equation [20] are:

- σ: porosity of the perforated plate,
- *d*: hole diameter,
- *e*: thickness of the perforated plate
- $k=\omega/c$: wavenumber,
- $\upsilon=\mu/\rho$: kinematic viscosity,
- M_r Mach number of the grazing flow and M_t Mach number if exists a through flow,
- C_D: Discharge coefficient
- $\delta_{re}=0.2d+200d^2+16000d^3$: end correction for the resistance
- $f_{\mathrm{int}}=1-1.47\sqrt{\sigma}+0.47\sqrt{\sigma^3}$: interaction between holes
- $|u_n|=|p|/\left(\rho c\sqrt{r^2+\chi^2}\right)$: incident acoustic velocity
- $F(\mu)=1-4J_1(Kd/2)/(Kd.J_0(Kd/2))$,
- J_0 and J_1 are the zeroth and first order Bessel function of the first kind,
- $\mu'=2.179\mu$: absolute viscosity for highly conducting wall
- $K=\sqrt{-j\omega/\upsilon}$ and $K'=\sqrt{-j\omega/\upsilon'}$: Viscous Stokes wavenumbers inside the holes.

For further details see Elnady [6]

3.2 Discharge Coefficient

The discharge coefficient plays a major role in impedance prediction. This coefficient takes into account for the *vena contracta* in each orifice. Elnady & al.[6] measured this coefficient by DC flow resistance in several perforated plates. For the present study, with perforated plates of a 2.5mm thickness, the discharge coefficient is of the order of 0.9 whatever the orifice diameter (from 0.6 to 5 mm).

3.3 Non-linear model impedance

For high SPL incident wave, i.e. for high acoustic particle displacement, non-linear effect can occur. Elnady & al.[6] propose the following additional term for the model impedance :

$$\left[\frac{(1-\sigma^2)}{\sigma^2C_D^2}\frac{1}{2c}\left(1-\frac{j}{3}\right)\right]|u_n|. \qquad [21]$$

The difficulty is that, for a given incident SPL, the acoustic velocity depends on the impedance but the impedance is a function of the acoustic velocity.

Hence, an iterative procedure must be followed to determine the acoustic non linear impedance. As an alternative, Elnady & al. [6] give the following resolution.
The surface impedance can be written with a linear part A and with a non-linear part B :

$$z = A + B|u_n|, \qquad [22]$$

with $|u_n| = |p|/\rho c|z|$, the previous equation becomes:

$$z = A + C|z|^{-1}, \qquad [23]$$

where $C = \frac{B|p|}{\rho c} = \left[\frac{(1-\sigma^2)}{\sigma^2 C_D^2}\frac{1}{2c}\left(1-\frac{j}{3}\right)\right]\frac{|p|}{\rho c}$.

In order to solve this equation let $z = Qe^{i\varphi}$, then:

$$Qe^{i\varphi} = A + CQ^{-1}. \qquad [24]$$

Multiplying this equation by its conjugate, we obtain:

$$Q^4 - |A|^2 Q^2 - 2[\mathrm{Re}\{A\}\mathrm{Re}\{C\} + \mathrm{Im}\{A\}\mathrm{Im}\{C\}]Q - |C|^2 = 0. \qquad [25]$$

Equation [25] has only one real solution which is find numerically.
Finally the argument φ of the impedance is obtained by:

$$\varphi = \arg\left(A + CQ^{-1}\right). \qquad [26]$$

3.4 Perforated plate with wiremesh
The impedance of a perforated plate associated with a wiremesh is not very documented in the literature. According to Malmary [8] experimental studies on the topic show that the resulting impedance is little sensitive to the acoustic velocity and to the grazing flow. For that reason, a perforated plate with a wiremesh is described here by a linear impedance.
In the present study the wiremeshes are only characterized by a resistance evaluated experimentally R_{DC}. This value is then simply added to the resistance of the perforated plate:

$$r_{perforated.plate+wiremesh} = r_{plate} + \frac{R_{DC}}{\sigma}. \qquad [27]$$

4. Experimental Set-Up

4.1 Test Bench
For the present study, the flow test bench developed at LAUM laboratory is used. An air scroll compressor provides a stable inflow up to a mass flow rate of about 500 kg/h to the test section through a water cooler, a calming chamber and a muffler insuring clean and silent inflow. Two acoustic sources are mounted on either side of the test section where the airflow can go through. Four upstream and four downstream ¼" microphones are mounted flush on pipes of 30mm diameter on each side of the test mock-up.

4.2 Test mock-up
We defined a test mock-up where the porosity and the length of the perforated plate and the length of the quarter wave cavities vary in a wide range. The inner diameter is fixed to d_1=30 mm and the outer to d_2=50mm (Figure 4). The central perforated pipe is removable with a 120 mm maximum perforated length. The thickness of the perforated pipe was e=2.4 mm and the hole diameters for the pipes of 4% and 30% of porosity was 3mm and 4mm for the pipe of 60% of porosity. On each side, a thin cylinder slides on the perforated pipe in order to adjust the perforated length. Two thick cylinders slide on the previous ones in order to choose the quarter wave length cavities. Finally, the wiremeshes can be inserted into the internal perforated tube.

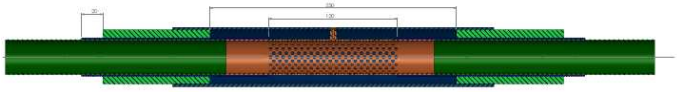

Figure 4 : Test mock-up

The range of the variable parameters is given in table 4.

Porosity	4% - 30% - 60% (3 pipes)
Wiremesh (Resistance in Rayls MKS at 20°C)	0 – 50 - 230 – 330 – 490 – 940
L_p	from 0.75*d1 (22.5mm) to 4*d1 (120mm)
L_1 and L_2	5*d1-L_p/2

Table 4 : Variable parameters

4.3 Scattering matrix measurements
The test unit is characterized by its scattering matrix obtained with incoming and outcoming wave decomposition:

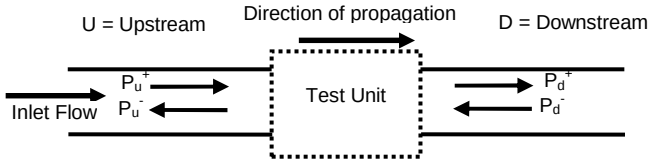

Figure 5 : A two-port acoustic system
The scattering matrix is composed of four elements, two complex transmission coefficients and two complex reflection coefficients:

$$\begin{pmatrix} P_d^+ \\ P_u^- \end{pmatrix} = \begin{pmatrix} T^+ & R^- \\ R^+ & T^- \end{pmatrix}\begin{pmatrix} P_u^+ \\ P_d^- \end{pmatrix} \qquad [28]$$

Two independent states are necessary to full determine this system. A two sources method is here employed to ensure the independency of the two states.

5. Results

The objective of this study is to test a range of classical configurations and particularly their sensitivity to flow and high SPL: an expansion chamber, and associated tuned designs to improve their acoustical performances. All of this is well described for example by Munjal & al. [9].

5.1 Simple Expansion Chamber

With the present mock-up, we tested first a simple expansion chamber of L=240mm length. The area ratio $N = S_2/S_1$ is equal to 2.78. In this configuration there was no flow through the chamber and the level of acoustic excitation was about 100dB SPL (re 20µPa).

The four parameters (modulus) are compared with the non linear model versus the normalized frequency kL/π (Figure 6). The porosity is set to 100% to describe in the model the absence of a perforated screen.

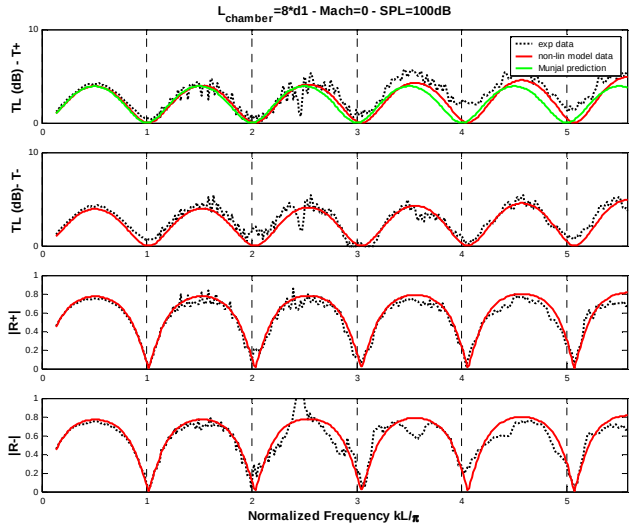

Figure 6 : Simple Expansion Chamber

The usual result for this configuration shows several bumps where maxima of attenuation occur at $kL/\pi = (2n-1)/2$ and troughs of attenuation at $kL/\pi = n$. At the first line (the common TL curve associated with the T^+ coefficient), the prediction of Munjal [9] is added to the results:

$$TL = 10.\log\left[1+0.25\left(N-\frac{1}{N}\right)^2 \sin^2(kL)\right] \qquad [29]$$

The levels are very similar but we can already observe a little shift toward high frequencies at the location of troughs on the experimental data. Our analytical model predicts this little shift that could be related to the fact that our geometry is similar to a "short resonator" configuration as defined by Sullivan [10], exhibiting interaction of upstream and downstream evanescent modes.

5.2 Expansion Chamber with ¼ waves resonators

The usual way to optimize the acoustical performance of the expansion chamber is to tune the quarter wave cavities length in order to have the resonances located at the troughs of the expansion chamber's attenuation (Munjal & al. [9]). In this case:

$L_1 = L/4 = 2d_1$, $L_p = L/4 = 2d_1$ and $L_2 = L/2 = 4d_1$

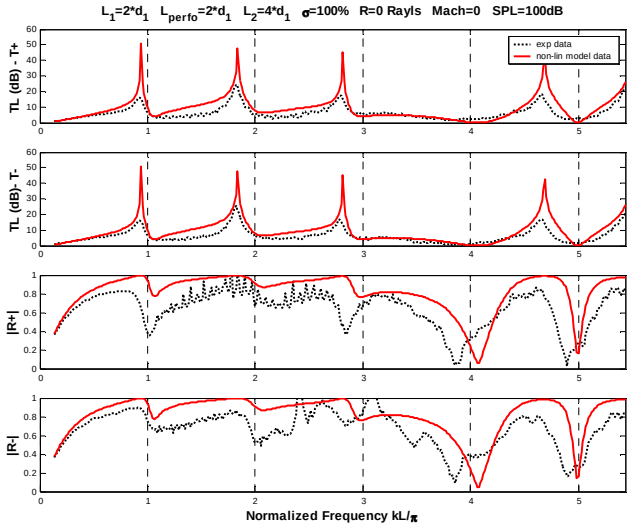

Figure 7 : Expansion Chamber with ¼ wave resonators

On Figure 7, both experimental and model data show a great attenuation at the quarter wave resonances but at high frequencies they are not located at $kL/\pi = n$ as Munjal & al. [9] predict it in a first approximation. The prediction of Munjal & al. would be certainly better if interaction of added lengths of the extended inlet and outlet were taken into account. Indeed for a ratio $L/d_1 = 20$, i.e. for a configuration less sensitive to added lengths, the resonances are close to $kL/\pi = n$ (Figure 8).

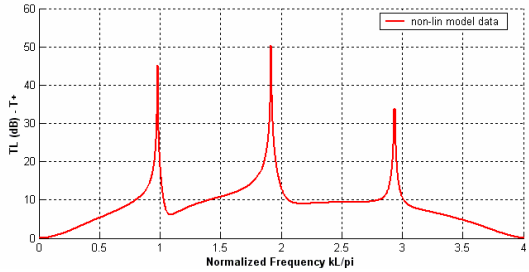

Figure 8 : Longer Chamber with ¼ Wave resonators

5.3 Non-linear acoustical effect

A perforated tube of 4% of porosity is added to the previous configuration. No flow is imposed and three levels of acoustic excitations were applied: 100 – 135 and 150dB. For each level the linear model is added in green to the plots as a reference.

Due to the presence of the perforated tube, the locations of the resonances of the quarter wave resonators are no longer near $kL/\pi = n$ (Figure 9).

For a low level excitation the two models are stacked and a good agreement is observed with experimental data. As the level of excitation increases, the maxima are attenuated and well

predict by the non-linear model (Figure 10 and Figure 11).

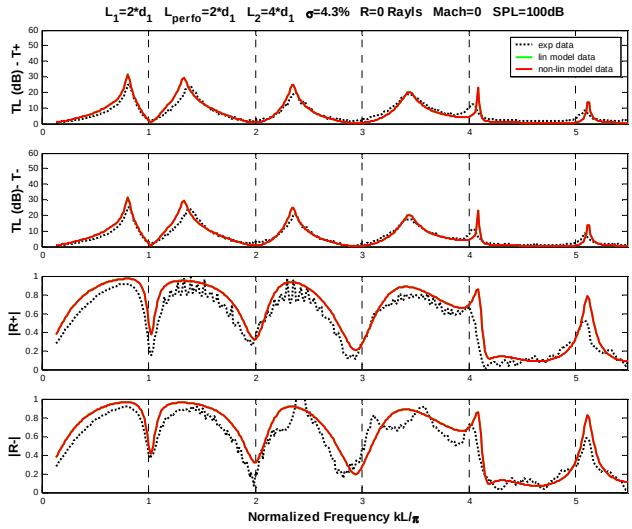

Figure 9 : Low-Level excitation (100dB)

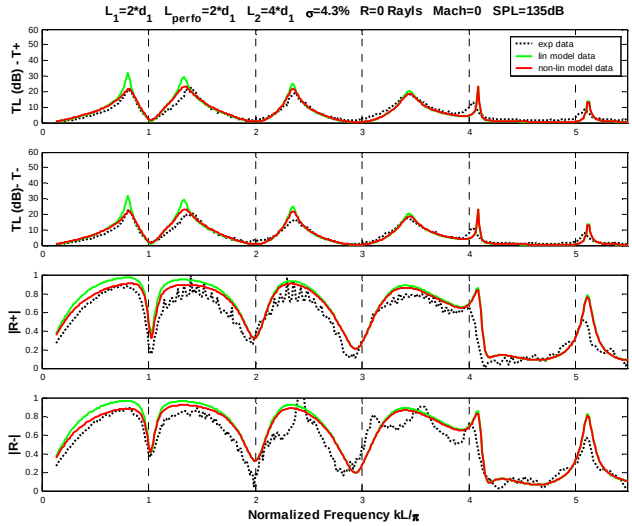

Figure 10 : Medium-Level excitation (135 dB)

On Figure 12, the computed normalized impedances for the two models and for the three levels of excitation are compared. The increase of the level excitation induces a great rise of the resistance and above all at low frequencies where the acoustic velocities are high. On the other hand, the reactances are almost not affected by the high sound pressure level. These phenomena are widely reported in existing literature.

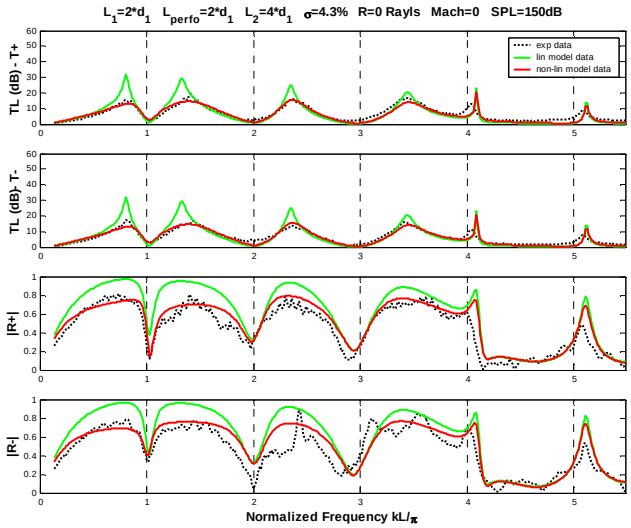

Figure 11 : Medium-Level excitation (150 dB)

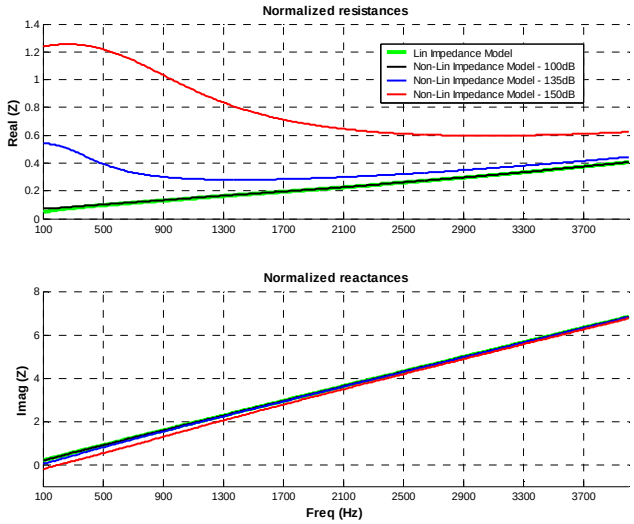

Figure 12 : Computed Normalized Impedances

5.4 Wiremesh effect

The effect of the presence of wiremesh against the internal face of the perforated tube is tested with the 60% porosity pipe.

First, the Figure 13 presents the results without flow and without wiremesh. In this case, the location of maxima tends to go to those observed for the open chamber – i.e. without perforated pipe (see Figure 7). The levels obtained with the model are overestimated compared with the experimental data. This overestimation is already observed without perforated pipe (Figure 7).

When the wiremesh is added (Figure 14), the peak levels are strongly attenuated and the reflection coefficients slightly decrease. This effect is correctly reproduced by the impedance model (Figure 15) even if some discrepancies appear on the modulus of the reflexion coefficients.

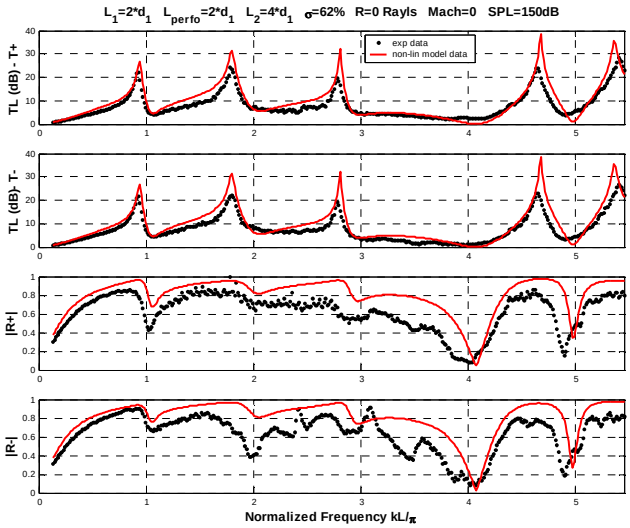

Figure 13 : R=0

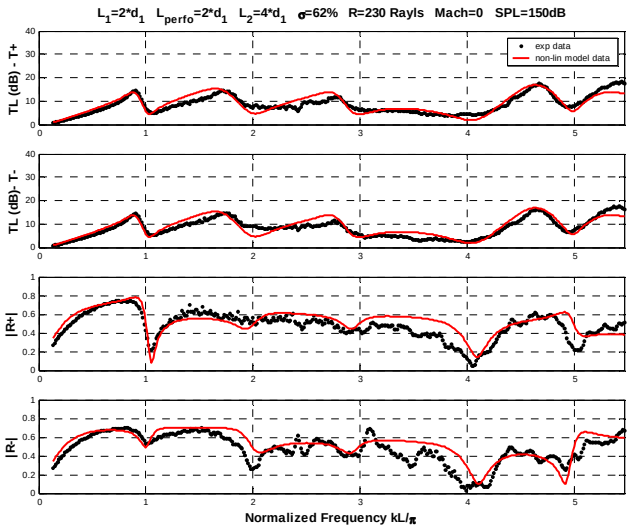

Figure 14 : R=230 Rayls

5.5 Mean Flow Effect

The effect of flow on the acoustic muffler performances is tested with the same perforated pipe (porosity 62%) as previous associated with the 230 Rayls wiremesh.

For Mach numbers M=0.1 and M=0.2, and with R=230 Rayls for the modelling of the resistance, the computed values agree quite well with the experimental ones (Figure 15 and Figure 16). Furthermore, with the increase of the flow rate, the transmission loss associated with the coefficient T+ slightly decreases whereas the reverse transmission loss (T-) tends to increase. This is also well predicted by the present model.

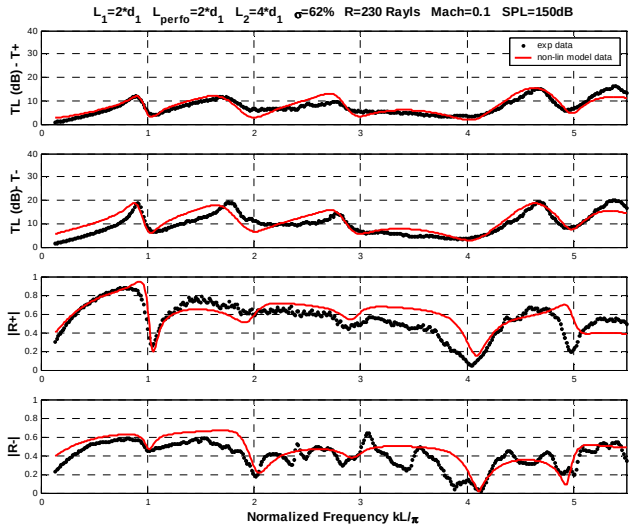

Figure 15 : M=0.1

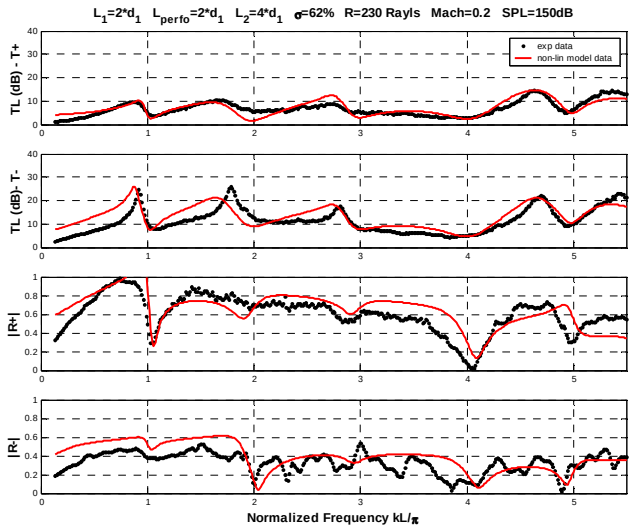

Figure 16 : M=0.2

6. Conclusions

In this paper, an analytical model is presented and used to compute the scattering matrix of a reacting dissipative silencer.

A radial variation of pressure is taken into account on either side of the perforated tube. The hydrodynamics modes and the Kutta condition are also considered. Moreover this model is associated with a complete impedance model that takes into account high pressure level, i.e. the non-linear effects that appear when high acoustic velocities occur through the orifices of the perforated tube.

The proposed approach is extensively validated with experimental data for the complete scattering matrix and allows to describe precisely how the acoustical performance of very wide spread mufflers are modified in real world applications by flow and high

incident sound pressure levels. This leads to a good confidence for using this very tractable model during engineering process.
Further efforts should be done on the impedance model in particular for highly porous screen, effect of a porous material against the screen and to obtain experimental results at higher mach numbers since these conditions are in the scope of the present approach.

7. References

[1] Munjal, M. L. Acoustics of Ducts and Mufflers With Application to Exhaust and Ventilation System Design. 1er éd. Wiley-Interscience, 1987.

[2] Y.Aurégan, A.Debray, et R.Starobinski. “low frequency sound propagation in a coaxial cylindrical duct: application to sudden area expansions and to dissipative silencers.” Journal of Sound and Vibration 243, n°. 3 (Juin 7, 2001): 461-473..

[3] Aurégan, Y., et M. Leroux. “Failures in the discrete models for flow duct with perforations: an experimental investigation.” Journal of Sound and Vibration 265, n°. 1 (Juillet 31, 2003): 109-121.

[4] Dokumaci, E. “Effect of sheared grazing mean flow on acoustic transmission in perforated pipe mufflers.” Journal of Sound and Vibration 283, n°. 3 (Mai 20, 2005): 645-663.

[5] Marx, David, Yves Aurégan, Hélène Bailliet, et Jean-Christophe Valière. “PIV and LDV evidence of hydrodynamic instability over a liner in a duct with flow.” Journal of Sound and Vibration 329, n°. 18 (Août 30, 2010): 3798-3812.

[6] T. Elnady, H. Bodén, “On the modelling of the Acoustic Impedance of perforates with flow”, The Marcus Wallenberg Laboratory for Sound and Vibration Research, AVE, KTH, Stockholm, Sweden, 2004.

[7] Y. Aurégan "Low frequencies acoustical behaviour of multi-cell systems in flow duct" Internal Report LAUM/OG/2000/1.

[8] C. Malmary, "Etude théorique et expérimentale de l'impédance acoustique de matériaux en présence d'un écoulement d'air tangentiel", Thèse de Doctorat de l'Université du Maine, Sept 2000.

[9] M.L. Munjal, A.G. Galaitsis, I.L. Vér, " Noise and Vibration Control Engineering: Principles and Applications", Second Edition, Chapter 9, István L. Vér, Leo L. Beranek, 2007

[10] Sullivan, Joseph W., et Malcolm J. Crocker. “Analysis of concentric-tube resonators having unpartitioned cavities.” *The Journal of the Acoustical Society of America* 64, n°. 1 (Juillet, 1978): 207-215.